Available online at www.sciencedirect.com
ScienceDirect
Applied Surface Science 253 (2007) 6289–6294
applied surface science
www.elsevier.com/locate/apsusc

Substrate influence in electron–phonon coupling measurements in thin Au films

Patrick E. Hopkins, Pamela M. Norris *

Microscale Heat Transfer Laboratory, University of Virginia, Charlottesville, VA 22904-4746, United States

Available online 27 January 2007

Abstract

Accurate understanding and measurement of the energy transfer mechanisms during thermal nonequilibrium between electrons and the surrounding material systems is critical for a wide array of applications. With device dimensions decreasing to sizes on the order of the thermal penetration depth, the equilibration of the electrons could be effected by boundary effects in addition to electron–phonon coupling. In this study, the rate of electron equilibration in 20 nm thick Au films is measured with the Transient ThermoReflectance (TTR) technique. At very large incident laser fluences which result in very high electron temperatures, the electron–phonon coupling factors determined from TTR measurements deduced using traditional models are almost an order of magnitude greater than predicted from theory. By taking excess electron energy loss via electron-substrate transport into account with a proposed three temperature model, TTR electron–phonon coupling factor measurements are more in line with theory, indicating that in highly nonequilibrium situations, the high temperature electron system looses substantial energy to the substrate in addition to that transferred to the film lattice through coupling.

PACS : 79.20.Ds; 73.50.−h; 73.61.−r; 72.10.Di; 66.70.+f; 73.63.Bd; 65.80.+n

Keywords: Electron–phonon coupling; Two temperature model; Thin films; Ultrashort pulsed laser heating; Nonequilibrium

1. Introduction

The occurrence of electron–phonon nonequilibrium in metal films is an important consideration in many pulsed laser applications. In material manufacturing applications such as ablation and laser processing of metals, knowledge of the electron–phonon coupling is critical for accurate modeling [1,2]. This nonequilibrium must be considered in the mirrors and highly reflective surfaces that comprise pulsed laser systems; electron nonequilibrium at rear mirror surfaces could lead to more rapid degradation and warping of mirror contacts due to thermal processes [3,4]. The need to understand nonequilibrium electron–phonon processes extends even to high frequency solid state devices [5]. As the operating frequencies of these devices increase and characteristic sizes decrease, the electric field generated from the gate potentials can reach levels high enough to impart enough force on the electron system to throw it out of equilibrium with the lattice. The need to understand and measure the electron–phonon relaxation in materials typical in these devices is critical for the advancement of engineering and design of solid state technology. Nonequilibrium electron processes, such as electron–phonon relaxation, are most efficiently observed with pulsed laser measurement techniques.

Electron–phonon nonequilibrium resulting from pulsed laser heating can be divided into three characteristic time intervals [6,7]. The earliest of the time intervals, the duration of which is called the relaxation time, τ_{ee}, is typically on the order of 10–100 fs for metals [8]. This time represents the time it takes for the excited electrons to relax into a Fermi distribution through e–e (electron–electron) collisions, which dominate e–p (electron–phonon) collisions during this time interval. Ballistic transport of the electrons also occurs over this time and the depth to which the electrons ballistically travel is significantly larger than the optical penetration depth in s- and p-band metals [6,9]. Once equilibrium is achieved within the electron system, the higher temperature electrons transmit energy to the lattice

* Corresponding author at: Department of Mechanical and Aerospace Engineering, University of Virginia, P. O. Box 400746, Charlottesville, VA 22904-4746, United States Tel.: +1 434 924 6295.
E-mail address: pamela@virginia.edu (P.M. Norris).

0169-4332/$ – see front matter © 2007 Elsevier B.V. All rights reserved.
doi:10.1016/j.apsusc.2007.01.065

through e–p scattering processes as the electrons conduct energy deeper into the film away from the optically excited region [10,11]. The e–p interactions eventually lead to the two subsystems reaching an equilibrium temperature within a time determined by the specific heats of the systems and the electron–phonon coupling factor [12]. This thermalization time, τ_{ep}, is dependent upon the carrier density in the penetration depth of the laser, which is substrate dependent [10]. Thermalization time is typically on the order of one picosecond for metals, and is inversely related to the electron–phonon coupling factor [13]. Once e–p equilibrium is achieved, thermal transport is accurately given by Fourier's law as the thermal energy is transmitted deeper into the film at a rate proportional to the thermal conductivity of the material.

This e–p equilibration in Au films has been extensively studied [4,6,14–16]. Smith and Norris studied electron–phonon coupling in Au films at electron energies far below the Interband Transition Threshold (ITT); i.e. only electrons undergoing intraband transitions participate in electron–phonon energy transfer [14]. Hohlfeld et al. studied electron–phonon coupling in Au films of various thicknesses, with various fluences, using energies at and around the ITT, and measured the same rate of electron–phonon coupling as Smith and Norris—2.2×10^{16} Wm^{-3} K^{-1} [6]. This work also showed that in Au films ballistic electron transport can extend over 100 nm from the sample surface (defining a thermal penetration depth), creating homogeneously heated films in which cooling is dominated by e–p coupling [6]. In thicker films, the cooling from the optically excited region is complicated by both e–p coupling and diffuse electron transport into deeper regions of the film beyond the reach of ballistic transport.

The aim of this paper is to investigate substrate interference in e–p coupling measurements in 20 nm thick gold films. Electron–phonon coupling measurements on homogenously heated Au films in the current study are shown to be, in some cases, almost an order of magnitude higher than the accepted rate of electron–phonon coupling in Au. This discrepancy is observed in high temperature s-band electrons undergoing intra-conduction-band transitions. This discrepancy, however, diminishes when the increased energy loss of the electron system around the film/substrate boundary is taken into account in the calculations.

2. Experimental description

The rate of electron–phonon equilibration in 20 nm Au films on Si and glass (predominantly SiO_2) substrates was tested with the Transient ThermoReflectance (TTR) technique. The TTR technique employs an ultrashort pump pulse that is focused to a small spot on the surface of the metallic film that, upon absorption of the incident photons by the electrons in the metal, creates a temperature rise in the electrons of the film. This change in temperature of the film produces a proportional change in the optical reflectivity, which is dependent on the magnitude of the electron temperature and the specific electronic transitions excited during the heating event [14,17,18]. The change in the reflectivity is measured with a time-delayed probe pulse which is focused onto the film so as to overlap spatially with the pump pulse. The primary output of the laser systems utilized in this work emanates from a Coherent RegA 9000 amplifier (seeded with a Coherent MIRA 900 oscillator) operating at a 250 kHz repetition rate with about 4 μJ per pulse and a 150 fs pulse width at 800 nm (1.55 eV, which is below the 2.15 eV ITT for Au indicating that intraband transitions will dominate thermal transport). The 800 nm pulses were split at a 9:1 pump to probe ratio. The pump beam, modulated at 125 kHz, was focused down to a 100 μm radius spot size to achieve a maximum of 15 Jm^{-2} fluence. The probe beam was focused to the middle of the pump beam on the Au surface to achieve a pump to probe fluence ratio of 30:1 at the maximum pump fluence. The radii of the pump and probe beams were measured with a sweeping knife edge and the phase of the reflectance was used for data correction, as outlined in the references [19].

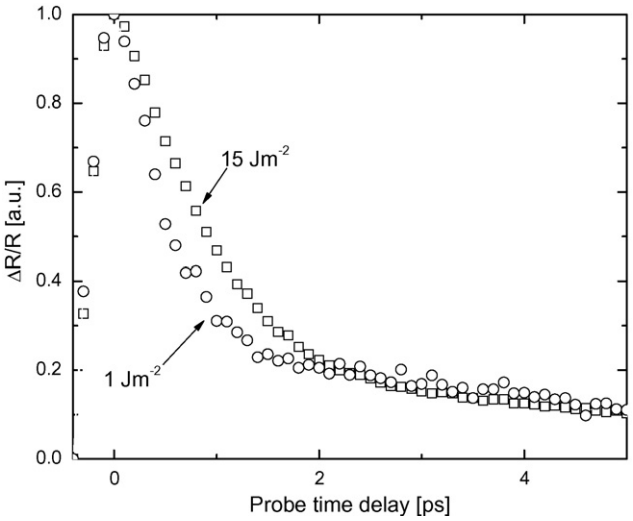

Fig. 1. Phase corrected TTR data on a 20 nm Au/glass sample taken at two laser fluences. The data is normalized at the peak reflectance to show the difference in cooling profiles of the electron systems during the first few picoseconds after laser heating. The initial time (t_0) is defined at time of peak reflectance.

Phase corrected TTR data for the Au/glass film taken at 1.0 and 15 Jm^{-2} incident laser fluence are shown in Fig. 1. These data are normalized at the peak reflectance to observe the difference between the electron cooling profiles at these different fluences, and $t = 0$ is defined as the time at maximum reflectance. Although the magnitude of $\Delta R/R$ is much greater after a 15 Jm^{-2} pump pulse than after a 1.0 Jm^{-2} pump pulse, the shape of the cooling profile after the maximum electron temperature is what is related to the rate of electron–phonon equilibration, therefore the normalization of the data is for clear comparison between the two data sets. The majority of the electron energy loss to the phonons occurs within the first 1–2 ps. Differences in the data are seen within 2 ps after the maximum reflectance, indicating a difference in the cooling rate of the electron system during electron–phonon equilibration.

The nonequilibrium temperature induced in the TTR experiments can be accurately predicted with the Two Temperature Model (TTM) [8,20]. This model, given by Eqs. (1) and (2), describes the rate of energy exchange between

the electrons and phonons in a metallic film:

$$C_e(T_e)\frac{\partial T_e}{\partial t} = \frac{\partial}{\partial x}\left(k_{eff}(T_e, T_l)\frac{\partial T_e}{\partial x}\right) - G(T_e - T_l) + S(x,t), \quad (1)$$

$$C_l\frac{\partial T_l}{\partial t} = G(T_e - T_l). \quad (2)$$

where C_e is the temperature dependent electronic heat capacity defined as a product of the Sommerfeld constant and the electron temperature, $C_e = \gamma T_e$ [21], G is the electron–phonon coupling factor [15], $S(x, t)$ is the laser source term which describes the radiation energy absorbed by the electron system [12], $k_{eff}(T_e, T_l)$ is the effective electron thermal conductivity that accounts for e–e and e–p scattering [22], and C_l is the lattice heat capacity taken at 300 K [23], which is assumed to be temperature independent due to minimal lattice heating during the first few picoseconds of laser heating. The energy transport processes modeled by the TTM can be assumed one dimensional when the heated area is much greater than the film thickness.

Since the Au films in this study are thinner than the thermal penetration depth (~100 nm), they are assumed to be homogeneously heated after τ_{ee}, meaning the electron temperature difference between the front and rear surfaces of the film can be assumed negligible ($\partial T_e/\partial x = 0$) [6]. Therefore, Eq. (1) is simplified to:

$$C_e(T_e)\frac{\partial T_e}{\partial t} = -G(T_e - T_l) + S(t), \quad (3)$$

where the source term is now simplified from its traditional form [12] to:

$$S(t) = \frac{0.94(1-R)F}{t_p d}\exp\left[-2.77\left(\frac{t-2t_p}{t_p}\right)^2\right], \quad (4)$$

where the fluence F and pulse width t_p are incident laser pulse properties, the reflectivity R is a thickness and substrate dependent material property [24], and an appropriate choice of the film thickness d ensures that all the incident laser energy is absorbed in the electron system. Using the film thickness d as the characteristic length in which the incident fluence is absorbed in the film also assumes that some degree of ballistic transport will be blocked (assuming $d <$ ballistic range) and reflection at the film/substrate boundary results in a higher energy density within the film [6]. This calculation assumes total reflection of the electron energy back into the depth of the film with spatial homogeneity.

Eqs. (2) and (3) are coupled ordinary differential equations describing the electron and lattice temperatures and they are solved numerically to generate electron and lattice temperature profiles. These profiles are then fit to reflectance data using the fitting procedure and nonlinear intraband reflectance model derived by Smith and Norris [14]. The model is fit to the first 2.0 ps of data after the transient peak to attain the minimum error. This corresponds to the time when the majority of the e–p coupling occurs, however, excellent agreement between the model and the data is observed for several picoseconds after the peak. The best fit G is obtained at the minimum error between the data and the fit, typically less than 1% in this study.

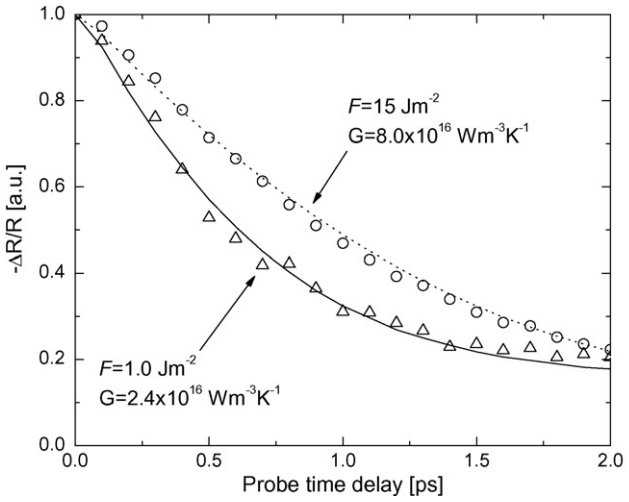

Fig. 2. TTM fit to the first 2.0 ps of the data in Fig. 1. The best fit resulted in drastically different G's for the two laser fluences.

Fig. 2 shows the TTM with the best fit values for G as determined from TTR data taken at both 1.0 and 15 Jm^{-2} fluence. These data show noticeably different cooling profiles, with the only variation between the measurements being the incident laser fluence. With 1.0 Jm^{-2} fluence, G was determined to be 2.4×10^{16} Wm^{-3} K^{-1}, yet with a much higher fluence of 15 Jm^{-2} the best-fit value of G was almost a factor of four larger, 8.0×10^{16} Wm^{-3} K^{-1}. The increased laser fluence causes an increase in electron temperature which creates a subsequent increase in G predicted by [25]:

$$G(T_e, T_l) = G_{RT}\left[\frac{A_{ee}}{B_{ep}}(T_e + T_l) + 1\right], \quad (5)$$

where G_{RT} is the room temperature value of G (experimentally observed in Au, $G = 2.2 \times 10^{16}$ Wm^{-3} K^{-1}) [25], and A_{ee} and B_{ep} are the electron–electron and electron–phonon scattering coefficients, respectively. The values of these scattering coefficients, $A_{ee} = 1.2 \times 10^7$ K^{-2} s^{-1} and $B_{ep} = 1.23 \times 10^{11}$ K^{-1} s^{-1} [26–28], are weakly dependent on temperature in Au [29]. The predicted maximum electron temperature from the TTM associated with the 15 Jm^{-2} incident fluence (along with the experimentally determined value of the e–p coupling factor, 8.0×10^{16} Wm^{-3} K^{-1}, and taking into account the change in optical absorption between the Au/Si and Au/glass samples [24]) is ~2600 K. At this temperature, G is predicted as 2.8×10^{16} Wm^{-3} K^{-1} via Eq. (5), still significantly less than the measured G. Eq. (5) was derived assuming that electron–electron scattering can affect electron–phonon coupling. Other calculations on the temperature dependency of electron–phonon coupling in Au assume that electron–electron scattering may not play a role in G in the temperature range predicted in this study [30,31]. These works predict a constant G at temperatures below ~3500 K and then a steep nonlinear increase due to d-band electrons populating the Fermi surface

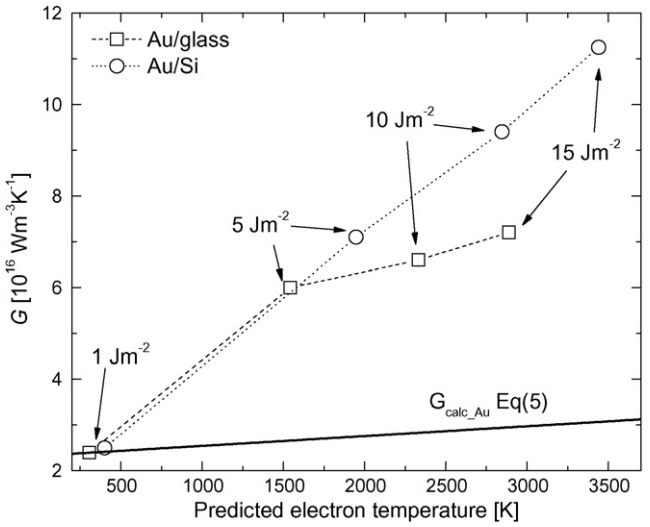

Fig. 3. Best fit G for 20 nm Au on Si and glass at several different laser fluences. The large divergence of the measured G using the TTM from that predicted G using Eq. (5) could be a result of a nonequilibrium between the electrons and substrate causing another channel for energy transfer away from the electron system.

at higher temperatures. The increase in G observed from TTR experiments is so large compared to the increase predicted from Eq. (5) assuming electron–electron scattering effects that $G(T_e, T_l)$ calculated via Eq. (5) is essentially constant over the temperature range predicted in this study.

Fig. 3 shows values of G measured on the Au/glass and Au/Si samples as a function of the maximum electron temperature as predicted by the TTM best fit. The data were taken at four different fluences as depicted in the figure. At low temperatures ($\Delta T_e \sim 100$ K), G matches the value measured by previous groups [6,14] and predicted by Eq. (5). At high temperatures, the data indicate that the electrons and phonons are equilibrating at a much faster rate than predicted from Eq. (5). This could be a result of high temperature electrons at the film/substrate boundary loosing energy through electron-boundary scattering, thereby offering another mechanism of energy loss from the electron system.

3. Boundary scattering effects on G

By examining the trends between the two data sets in Fig. 3, some boundary scattering influence is qualitatively observed. If the measured value of G was only dependent on temperature, then results for the Au/glass and Au/Si samples would not diverge at high temperatures. However, the differing high temperature trends between the samples indicate that some properties of the boundary (which would differ based on differing properties between Si and SiO_2) could be affecting the measurements. The rate in which the G measurements increase with temperature is much greater in the Au/Si sample then the Au/glass sample. This is conceptually intuitive, since a semiconducting substrate like Si would be more apt to transfer energy away from the electron system than an insulting substrate like glass. The higher the electron temperature, the greater the rate of energy transfer between the electron system and substrate through electron-boundary scattering, thereby increasing the apparent electron–phonon coupling factor as determined with TTR technique. These trends were not seen by Hohlfeld et al. who examined Au films at various fluences around the ITT [6]. However, this channel of electron-substrate energy transfer could in fact still be present in their data but the large optical response associated with the interband transition could mask any effects of the free electron gas loosing energy to the underlying substrate [18].

In an attempt to quantify the amount of energy lost from the electron system due to electron boundary scattering, Eq. (3) must be modified to include a term accounting for this transport channel. Assuming that the boundary is the same temperature as the substrate, T_{sub}, which during the two picoseconds of nonequilibrium can be treated as constant at ambient assuming a minimal rise in lattice temperature [32], Eq. (3) is modified to take into account substrate energy loss:

$$C_e(T_e)\frac{\partial T_e}{\partial t} = -G(T_e - T_l) - \frac{M}{d}(T_e - T_{sub}) + S(t), \qquad (6)$$

where M represent the amount of energy loss by the electron system to the boundary via electron-boundary scattering. Eqs. (6) and (2) form a Three Temperature Model (3TM). In the case of the Au films in this study, the 3TM was used to examine electron-boundary effects on G in the first few picoseconds of nonequilibrium cooling, therefore phonon–phonon boundary scattering is neglected (which would cause a slight modification to Eq. (2) to account for phonon mediated thermal boundary conductance [33]). In addition, the 20 nm Au film was still considered homogeneously heated and therefore it is assumed that no thermal gradient is induced when electrons loose energy at the rear of the film. This is a valid assumption presuming that the film thickness is less than the electron–electron mean free path.

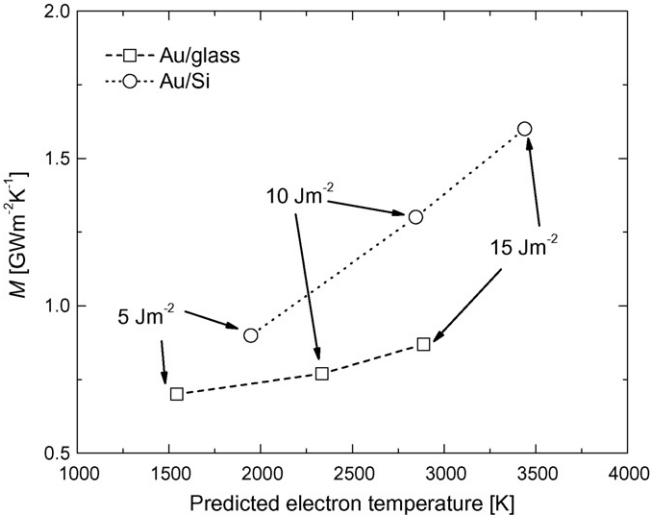

Fig. 4. Rate of energy loss from the electron system beyond e–p coupling, M, deduced from the 3TM applied to TTR data assuming a G temperature dependence in accordance with Eq. (5). The electron system energy loss is always greater on the semiconducting Si substrate than on the insulating glass substrate.

The 3TM was applied to the TTR data by varying M until the TTR best fit G matched that predicted by Eq. (5). The error associated with the G fit with the 3TM was on the same order as that with the TTM. The measurements associated with low electron temperatures ($F = 1.0\ \mathrm{Jm^{-2}}$) matched the predicted G so energy loss to the substrate was considered negligible ($M = 0$). However, in the higher temperature measurements, M ranged from 0.7 to 1.6 $\mathrm{GWm^{-2}\,K^{-1}}$ depending on the substrate and laser fluence. These results are shown in Fig. 4. Examining Fig. 3, these results are rather intuitive, as a higher value of G would correspond to a larger amount of energy lost to the substrate. In addition, the energy lost to the Si substrate is always greater than the energy lost to the glass substrate, quantitatively showing what was previously qualitatively discussed.

4. Analysis

The electron-boundary scattering results in a heat flux from the electron system to the underlying substrate. In this way, M can be treated as an electronic Kapitza conductance. Sergeev derived a relationship between the electronic Kapitza conductance (represented by σ_K^e in Sergeev's work), electron properties, and substrate properties [34,35]. This model predicts a Au/Si Kapitza conductance of $\sigma^e = 30\,\mathrm{MWm^{-2}K^{-1}}$, assuming the electrons and metal lattice are in thermal equilibrium. The temperature dependence in this calculation is solely based on substrate temperature ($T = 300$ K). Since σ_K^e was derived using assumptions in calculations of electron–phonon and electron-impurity scattering, these assumptions were valid for the minute differences in electron and substrate temperatures encountered in the applications of his model. This model was applied to experimental results from thermo modulation experiments on solid interfaces with nanosecond decay time constants, therefore, the electrons would be in equilibrium with the film phonons and the temperature drop between the electrons and substrate would be far less than the temperature drop in this current study.

The data and calculations in this work predict electron temperatures in the heated films as much as ~3000 K greater than the substrate temperature. This large nonequilibrium at the interface could increase interfacial thermal transport, as the experimental data implies. A better quantitative prediction for electron energy loss during nonequilibrium laser heating is achieved by examining the thermal properties of the system. As the electron system looses energy[†] via various processes, it relaxes back down to close to room temperature over τ_{ep}. The time it takes for these electrons to relax is related to $G_{measured}$ in the TTR experiments, and since the electron temperature is so elevated, τ_{ep} is a function of both C_e and the lattice heat capacity, C_l [13]. Considering that during this time electrons are loosing energy to the lattice in addition to other processes (such as electron-boundary scattering), G_{calc} (predicted by Eq. (5)) can be subtracted from the predicted total amount of energy lost by the electron system to determine the energy lost per unit volume per unit time by the electron system to processes other than electron–phonon coupling. Assuming that this volumetric heat transfer is homogeneous through the film thickness, the energy loss can be projected to the interface and the energy lost to processes other than electron–phonon coupling can be calculated from:

$$M = d\left[\frac{\gamma\left(T_{max}^2 - 300^2\right)\left(\gamma T_{max} + C_l\right)G_{measured}}{\gamma T_{max} C_l\left(T_{max} - 300\right)} - G_{calc}\right] \tag{7}$$

Eq. (7) estimates the energy loss from the electron system at the maximum electron temperature. Consider the Au/Si high fluence case where Eqs. (3) and (2) predict an electron temperature of 3440 K and $\gamma T_e = 214.2\ \mathrm{kJm^{-3}\,K^{-1}}$, $C_l = 2.5\ \mathrm{MJm^{-3}\,K^{-1}}$, $G_{measured} = 1.13 \times 10^{17}$, and $G_{calc} = 3 \times 10^{16}\ \mathrm{Wm^{-3}\,K^{-1}}$. This calculation yields $M = 1.97\ \mathrm{GWm^{-2}\,K^{-1}}$, which is in close agreement with the $1.6\ \mathrm{GWm^{-2}\,K^{-1}}$ rate of electron-substrate energy loss deduced from the 3TM. Fig. 5 shows the predicted M from Eq. (7) using $G_{measured}$ and T_{max} predicted from the TTM best fit along with M deduced from the TTR experiments and the 3TM. The agreement between Eq. (7) and the value deduced from measurements leads to promising conclusions that an increase in $G_{measured}$ beyond what is predicted from Eq. (5) could be a result of high temperature electrons loosing energy to the substrate. In the low temperature case, where $G_{measured} = G_{calc}$ using the 3TM with $M = 0$, Eq. (7) still predicts a relatively small amount of energy transfer out of the electron system via non e–p scattering processes. The value predicted from M in these low temperature cases when the

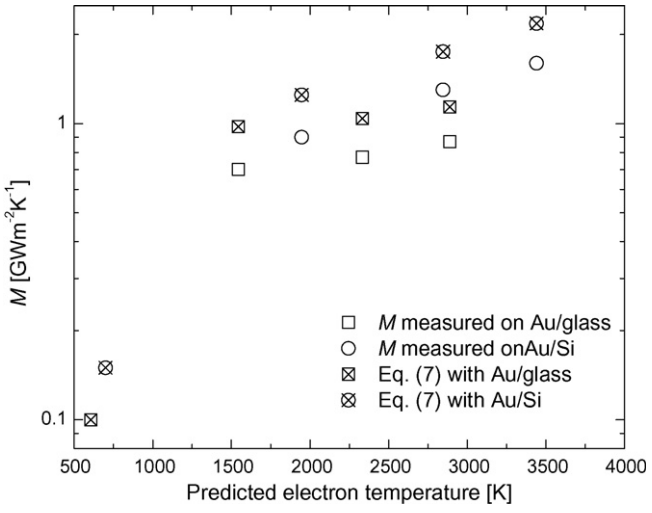

Fig. 5. Deduced M from TTR experiments using the 3TM compared to the calculated M using Eq. (7) and results using the TTM. Close agreement is shown between the high temperature data and calculations. In addition, at low electron temperatures when G measured with the TTM matched G_{calc} from Eqs. (5) to (7) predicts the rate of non e–p scattering energy transfer from the electron system to be close to that predicted from calculations for electron Kapitza conductance [34,35].

[†] The amount of energy lost by the electron system can be estimated by $C_e(T_e)(T_{max} - 300) = \gamma T_{max}^2 - \gamma 300^2$.

electron–phonon nonequilibrium is relatively small and within an order of magnitude as the predicted electronic Kapitza conductance from Sergeev's model assuming the electrons and phonons in the metal film are in thermal equilibrium. This indicates that although e–p scattering dominates at room temperature, other transport channels such as electron-boundary scattering could still be occurring with minimal effect on electron system energy loss. However, at much higher electron temperatures ($T_e \gg T_{room}$), electron-boundary scattering could play a significant role in energy transfer from the electron system.

5. Conclusion

In Au films with thicknesses on the order of the thermal penetration depth, nonequilibrium between the electrons in the metallic film and phonons at the metal/substrate boundary could lead to TTR measurements that are affected by electron energy loss to both the phonons in the metal film and those in the underlying substrate. A three temperature model was introduced to account for electron energy loss to the substrate. Using this model the electron–phonon coupling factor was measured and the excess energy loss from the electron system was observed for 20 nm Au films on glass and Si substrates. These values deduced from measurements agreed well with values calculated from simple energy transfer calculations, indicating that at high electron temperatures, electron–phonon energy transfer is not the only means of electron energy loss during the first few picoseconds after ultrashort pulsed laser heating.

Acknowledgements

This work would not have been possible with out financial support from the National Science Foundation Grant no. CTS-0536744 and Graduate Research Fellowship Program. The authors are greatly appreciative to Dr. Andrew Smith of the U.S. Naval Academy for his insightful discussions on this subject.

References

[1] D.S. Ivanov, L.V. Zhigilei, Phys. Rev. B 68 (2003), 064114.
[2] S.-S. Wellershoff, J. Hohlfeld, J. Gudde, E. Matthias, Appl. Phys. A 69 (1999).
[3] T.Q. Qiu, C.L. Tien, Int. J. Heat Mass Tran. 37 (1994) 2789–2797.
[4] T.Q. Qiu, T. Juhasz, C. Suarez, W.E. Bron, C.L. Tien, Int. J. Heat Mass Trans. 37 (1994) 2799–2808.
[5] A. Majumdar, K. Fushinobu, K. Hijikata, J. Appl. Phys. 77 (1995) 6686–6694.
[6] J. Hohlfeld, S.-S. Wellershoff, J. Gudde, U. Conrad, V. Jahnke, E. Matthias, Chem. Phys. 251 (2000) 237–258.
[7] I.H. Chowdhury, X. Xu, Numer. Heat Trans., Part A 44 (2003) 219–232.
[8] T.Q. Qiu, C.L. Tien, J. Heat Trans. 115 (1993) 835–841.
[9] S.D. Brorson, J.G. Fujimoto, E.P. Ippen, Phys. Rev. Lett. 59 (1987) 1962–1965.
[10] C.A.C. Bosco, A. Azevedo, L.H. Acioli, Appl. Phys. Lett. 83 (2003) 1767–1769.
[11] T.Q. Qiu, C.L. Tien, J. Heat Trans. 115 (1993) 842–847.
[12] P.M. Norris, A.P. Caffrey, R.J. Stevens, J.M. Klopf, J.T. McLeskey, A.N. Smith, Rev. Sci. Instrum. 74 (2003) 400–406.
[13] A.N. Smith, J.L. Hostetler, P.M. Norris, Numer.l Heat Trans., Part A 35 (1999) 859–873.
[14] A.N. Smith, P.M. Norris, Appl. Phys. Lett. 78 (2001) 1240–1242.
[15] J.L. Hostetler, A.N. Smith, D.M. Czajkowsky, P.M. Norris, Appl. Opt. 38 (1999) 3614–3620.
[16] J. Hohlfeld, J.G. Muller, S.-S. Wellershoff, E. Matthias, Appl. Phys. B 64 (1997) 387–390.
[17] H. Hirori, T. Tachizaki, O. Matsuda, O.B. Wright, Phys. Rev. B 68 (2003), 113102.
[18] P.E. Hopkins, J.M. Klopf, P.M. Norris, To Appear in Applied Optics.
[19] R.J. Stevens, A.N. Smith, P.M. Norris, Rev. Sci. Instrum. 77 (2006), 084901.
[20] S.I. Anisimov, B.L. Kapeliovich, T.L. Perel'man, Sov. Phys. JETP 39 (1974) 375–377.
[21] C. Kittel, Introduction to Solid State Physics, 7th Ed., John Wiley and Sons, Inc., New York, 1996.
[22] S.I. Anisimov, B. Rethfeld, SPIE 3093 (1997) 192–203.
[23] F. Incropera, D.P. DeWitt, Fundamentals of Heat and Mass Transfer, 4th Ed., Wiley and Sons, Inc., New York, 1996.
[24] F. Abeles, in: A.C.S.V. Heel (Ed.), Advanced Optical Techniques, North-Holland Publishing Co., Amsterdam, 1967, pp. 145–188.
[25] J.K. Chen, W.P. Latham, J.E. Beraun, J. Laser Appl. 17 (2005) 63–68.
[26] D.E. Gray, American Institute of Physics Handbook, 3rd Ed., McGraw Hill, New York, 1972.
[27] X.Y. Wang, D.M. Riffe, Y.-S. Lee, M.C. Downer, Phys. Rev. B 50 (1994), 8016-1019.
[28] A.H. MacDonald, Phys. Rev. B 44 (1980) 489–493.
[29] M. Kaveh, N. Wiser, Adv. Phys. 33 (1984) 257–372.
[30] A.N. Smith, P.M. Norris, 11th International Heat Transfer Conference, 5:241 (1998).
[31] Z. Lin, L. V. Zhigilei, High-Power Laser Ablation VI, Proc. SPIE 6261:62610U (2006).
[32] L. Shi, G.L. Huang, C. Lehane, D. Kim, H.S. Kwok, J. Swiatkiewicz, G.C. Xu, P.N. Prasad, Phys. Rev. B 48 (1993) 6550–6555.
[33] E.T. Swartz, R.O. Pohl, Rev. Mod. Phys. 61 (1989) 605–668.
[34] A.V. Sergeev, Phys. B 263/264 (1999) 217–219.
[35] A.V. Sergeev, Phys. Rev. B 58 (1998), R10199.